

Lawrence Berkeley National Laboratory

Recent Work

Title

MASS DISTRIBUTIONS IN THE REACTION OF 240 MeV ^{120}Sn WITH ^{197}Au

Permalink

<https://escholarship.org/uc/item/0x9468gb>

Authors

Kudo, H.

Moody, K.J.

Seaborg, G.T.

Publication Date

1984



Lawrence Berkeley Laboratory

UNIVERSITY OF CALIFORNIA

RECEIVED
LAWRENCE
BERKELEY LABORATORY
FEB 21 1984
LIBRARY AND
DOCUMENTS SECTION

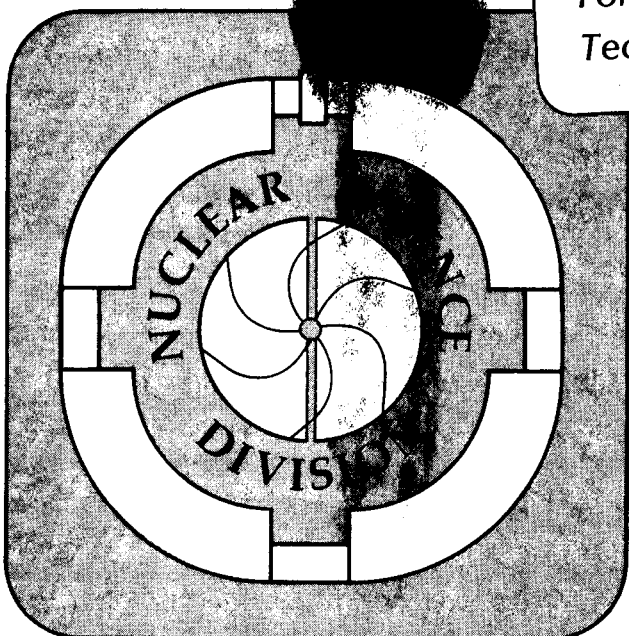
Submitted to Physical Review C

MASS DISTRIBUTIONS IN THE REACTION OF 240 MeV
 ^{12}O WITH ^{197}Au

H. Kudo, K.J. Moody, and G.T. Seaborg

January 1984

TWO-WEEK LOAN COPY
*This is a Library Circulating Copy
which may be borrowed for two weeks.
For a personal retention copy, call
Tech. Info. Division, Ext. 6782.*



LBL-17202
c.2

DISCLAIMER

This document was prepared as an account of work sponsored by the United States Government. While this document is believed to contain correct information, neither the United States Government nor any agency thereof, nor the Regents of the University of California, nor any of their employees, makes any warranty, express or implied, or assumes any legal responsibility for the accuracy, completeness, or usefulness of any information, apparatus, product, or process disclosed, or represents that its use would not infringe privately owned rights. Reference herein to any specific commercial product, process, or service by its trade name, trademark, manufacturer, or otherwise, does not necessarily constitute or imply its endorsement, recommendation, or favoring by the United States Government or any agency thereof, or the Regents of the University of California. The views and opinions of authors expressed herein do not necessarily state or reflect those of the United States Government or any agency thereof or the Regents of the University of California.

MASS DISTRIBUTIONS IN THE REACTION OF 240 MeV ^{12}O WITH ^{197}Au

H. Kudo,* K. J. Moody[†] and G. T. Seaborg^{††}

*On leave from Tokyo Metropolitan University, Tokyo, Japan
Department Chem. Faculty of Science, Niigata University,
Niigata, Japan

[†]Gesellschaft Für Schwerionenforschung mbH, Postfach 11 05 41.
6100 Darmstadt 11, West Germany

^{††}Nuclear Science Division, Lawrence Berkeley Laboratory,
University of California, Berkeley, California 94720

Abstract

The mass distributions of fission products and target-like products in the reaction of 20 MeV/A ^{12}C with ^{197}Au were determined radiochemically. The charge dispersions of the fission products were found to have Gaussian shapes with a width parameter ($2\sigma^2$) of 1.6 units and a most probable charge of $0.417 A + 1.4$. As for near- and above-target products, the charge dispersions of $A = 196 - 199$ had two peaks, one corresponding to a quasi-elastic process and the other corresponding to deeply inelastic and/or complete fusion processes. The cross sections of above-target products were larger than the values expected from simple evaporation calculations.

Keywords

NUCLEAR REACTION, 20 MeV/A $^{12}\text{C} + ^{197}\text{Au}$, mass distribution, charge dispersions, fission cross section, reaction mechanism, isomer ratios.

This work was supported by the Director, Office of Energy Research Division of Nuclear Physics of the Office of High Energy and Nuclear Physics of the U.S. Department of Energy under Contract No. DE-AC03-76SF00098.

I. Introduction

It is interesting to study how the reaction mechanisms in heavy ion induced reactions vary with incident projectile energy, especially for energies near the nuclear Fermi energy. In recent years, heavy ion beams of intermediate energy have become available for these experiments.

A radiochemical experiment usually aims at defining what occurs during a nuclear reaction by observing the change induced in a heavy target nucleus. These techniques were used in much of the early work with low energy reactions (a few MeV/A), where typical reaction processes are elastic scattering, quasi-elastic scattering, deeply inelastic scattering, complete fusion and incomplete fusion. Similarly, in high energy heavy ion reactions (hundreds of MeV/A or more), radiochemical measurements of forward-backward ratios, charge dispersions and mass distributions of residual nuclei¹⁻⁶ have helped develop the picture of a fast abrasive step followed by thermalization and de-excitation of the primary reaction products.

There is little published radiochemical work in the intermediate energy region. Most experiments performed at these energies have involved the measurement of the energy spectra of light emitted fragments which are interpreted with a moving source model⁷⁻⁹, a pre-equilibrium exciton model^{10,11}, the nuclear fireball model¹¹, etc. Symons et. al.¹¹ have used both a low energy model and a high energy model to try to explain the energy spectra of protons in the system of 20 MeV/A $^{16}\text{O} + ^{197}\text{Au}$. Egelhaaf et. al.¹² have concluded that, in the system of 20 MeV/A $^{20}\text{Ne} + ^{197}\text{Au}$, incomplete fusion and sequential decay occur in addition to complete fusion and

ordinary transfer reactions, and that other mechanisms do not contribute significantly.

In this work, we have examined the mass distribution of 20 MeV/A $^{12}\text{C} + ^{197}\text{Au}$ using precise radiochemical methods. We have chemically isolated both fission products and near-target products. Results have been compared with an evaporation calculation assuming the formation of a compound nucleus, and including pre-equilibrium processes via the exciton model.

II. Experimental

A. Irradiations

The experimental irradiations were performed at the Lawrence Berkeley Laboratory's 88-inch Cyclotron. The gold targets for most of the determinations consisted of uniform, self-supporting gold foils of 5.16 mg/cm^2 thickness, mounted between two pieces of 6.24 mg/cm^2 aluminum foil to completely collect both forward and backward recoil products. For experiments where products which decayed by alpha particle emission were measured (discussed below), the thickness of the gold foil varied from 1 mg/cm^2 to 2 mg/cm^2 , and the aluminum catcher foils were 1.8 mg/cm^2 in thickness, sufficient to stop complete fusion recoils.

The target foils were bolted to a copper block at the back of an electron-suppressed Faraday cup and were irradiated with 245 MeV $^{12}\text{C}^{5+}$ with an average intensity of about 20 electrical nanoamperes. The diameter of the beam spot was 10 mm, defined with an upstream graphite collimator. The irradiation times for each experiment varied from 5 minutes to 12 hours, depending upon the half lives of the nuclides which were of interest. The beam current entering the Faraday cup was measured

with an electrometer, and the integral was recorded periodically to permit accurate beam flux histories to be constructed.

To estimate the possible effect of secondary reactions on the measured reaction cross sections, a set of targets with different thicknesses between 1.0 mg/cm^2 and 5.16 mg/cm^2 were irradiated. It was found that, within statistics, there was no change in any of the reaction product cross sections as a function of target thickness. The evaluation of the contribution of secondary reactions in this reacting system was not a problem.

B. Chemical Separations

Each irradiated gold target with its aluminum cover foils was dissolved in aqua regia with an excess of HCl in a distillation flask containing carriers and/or tracers for the elements of interest. The elements characteristically present as fission products were separated with standard chemical procedures¹³. Brief comments on the separation schemes for the elements near gold are located in the Appendix at the end of this paper. Each run produced 3 to 10 samples. Chemical yields were obtained either by measuring the tracer activities, by weighing the carriers, or by comparison of the most intense activities with those measured from an unseparated target.

Almost all products at a significantly higher Z than that of the target were expected to recoil in the forward (beam) direction. In experiments designed to detect alpha-emitting polonium and astatine isotopes, thin gold foils were used (described above) that allowed these products to escape to the forward catcher foil. This was checked by surveying an unseparated target and forward foil for gamma-ray activity due

to ^{196}Pb and ^{198}Bi . Therefore, for measurements of polonium and astatine alpha activities, the forward aluminum catcher foil was melted on a copper disk and the volatile elements were collected on a copper foil cooled with liquid nitrogen or dry ice. Only alpha activity from polonium isotopes was observed. For more chemical details, see the Appendix.

C. Radioactivity measurements and data treatment

The activity of each product was determined by observing its characteristic gamma-rays except for ^{198}Po , ^{199}Po and ^{200}Po which were observed via their alpha activity. The gamma-ray spectrometer system was based on four Ge(Li) detectors equipped with pulse height analyzers. The photoelectric efficiencies of the detectors were determined as a function of gamma-ray energy for a number of well-defined geometries with a set of calibrated radionuclide sources. The energy resolutions (FWHM) of the detectors were 2.00, 2.05, 2.66 and 2.67 keV for the 1332 keV gamma-ray of ^{60}Co . The gamma-ray spectrum of each sample in the energy range $50 \text{ keV} < E < 2 \text{ MeV}$ was measured at a PHA gain of 0.5 keV/channel as a function of time for a total period of about two months for each run. For alpha activity measurements, a Si(Au) surface barrier detector was used. The efficiency of this detector was determined with a known amount of ^{210}Po source.

The gamma-ray spectral data were analyzed with the set of computer programs described in Ref. 14. These programs consist of a peak search, fitting and integrating program (SAMPO), a sorting program for decay curve construction (TAU1), and an interactive decay curve identification program (TAU2). Since the accuracy of the initial activities determined with TAU2 is defined by the accuracy of the isotope table used in

the identifications¹⁵, the intensity of each line was checked against more recent compilations^{16,17} to improve the reliability of these data. The end-of-bombardment activities were converted to cross sections taking into account both the appropriate chemical yield and the variation of the beam intensity during the irradiation. Whenever possible, the activities were corrected for precursor decay before the cross section calculation. If several gamma-rays of the same nuclide were observed, the cross section was calculated from the weighted average of all the corrected gamma-ray intensities.

III. Results and discussion

The cross sections of about 250 nuclides produced in the reaction of 20 MeV/A ^{12}C with ^{197}Au were determined and are tabulated in Table 1 and plotted in figure 1a. Table 1 also indicates whether or not a particular cross section is an independent yield, the experimental method by which it was observed, and the half life and principal gamma-ray energy and intensity used in the cross section calculation.

A. Fission products

Many of the observed fission products were members of the same mass chain, so the charge dispersion could be obtained. The shape of the charge dispersion was assumed to be Gaussian, $P(Z) = C \exp (-(Z_p - Z)^2 / 2\sigma^2)$. The most probable atomic number (Z_p) seems to be well-reproduced with the linear equation $Z_p = 0.417 A + 1.4$. The charge dispersions of all fission products (from $71 \leq A \leq 145$) were found to have similar values of the width parameter, $2\sigma^2 = 1.6$, except for mass numbers near those containing members with closed shells ($Z = 50$ or

$N = 82$). This is demonstrated in figure 2, where all the fission data are scaled and plotted on the same axes.

The width we observe here is rather large compared to those widths arising from processes at lower energy. In the reaction of 112 MeV ^{12}C with ^{197}Au , the width $2\sigma^2$ is 0.9¹⁸. The widths of the charge dispersions from the low energy fission of uranium range from 0.80 to 0.95^{19,20}. The broadening observed here results, in part, from the large variety of primary reaction products which will decay by fission, and partly from the high angular momentum of the fissioning nuclides. The dependence of the width parameter on excitation energy is thought to be small²⁰.

The data displayed in figure 2 gives a measure of the confidence with which the charge dispersions of the fission products can be described with the Z_p and width parameter detailed above. Using these values, the total chain yield for each mass number can be estimated from the available experimental data. The obtained mass distribution is plotted in figure 1b. In this figure, the solid line represents a Gaussian fit to the data points from $A = 71$ to $A = 145$. The peak of this mass distribution is at $A = 95.6$. The full width at half maximum is about 38, which is larger than those for the 126 MeV ^{14}N induced fission of ^{197}Au (FWHM = 30 ± 2)²¹, the 112 MeV ^{12}C induced fission of ^{197}Au (FWHM = 27)¹⁸, and the 105 MeV ^{12}C induced fission of ^{196}Pt (FWHM = 29.2)²², but is smaller than that for the reaction products from 391 MeV $^{40}\text{Ar} + ^{165}\text{Ho}$ (FWHM = 60)²³ for which it is assumed that there is a contribution due to other reaction processes. If we assume that the charge distributions of the fission products are the same as those of the fissioning nuclei, ignoring the possibility of neutron emission from the fission fragments, the "average" fissioning nucleus is near ^{191}Tl .

Blann¹⁸ measured a fission cross section of 0.9 b in the reaction of 112 MeV ^{12}C with ^{197}Au . Gordon et.al.²⁵ gave 1.28 b for the fission cross section in the reaction of 124 MeV ^{12}C with ^{197}Au , and Britt²⁶ gave 1.35 b for 126 MeV $^{12}\text{C} + ^{197}\text{Au}$. Wilke et.al.²⁴ have calculated fusion cross sections for the $^{12}\text{C} + ^{197}\text{Au}$ system at a variety of energies. For each of the reactions listed above, the calculated fusion cross section is larger than the observed fission cross section. The calculated fusion cross section in the 20 MeV/A $^{12}\text{C} + ^{197}\text{Au}$ system is 967 mb. From the fit to the charge-dispersion-corrected mass yield, shown in figure 1b, we obtain a fission cross section of 1700 mb. In this case there are two significant contributions to the fission cross section: fusion-fission and fission following nucleon transfer (sequential fission). If one proton with the velocity of the ^{12}C projectile is deposited in a ^{197}Au nucleus to make $^{198}\text{Hg}^*$, the excitation energy of the ^{198}Hg is about 27 MeV. The fission barrier of ^{198}Hg is only 22 MeV²⁷.

When the evaporation code ALICE²⁸, including pre-equilibrium processes, was used to model the reaction of 240 MeV $^{12}\text{C} + ^{197}\text{Au}$, the resultant fission cross section was 1700 mb. The initial exciton number was varied from 12 to 20, but this did not greatly affect the value of the fission cross section. This is a not unexpected result since, generally, fission occurs at rather low excitation energies, after several nucleon emissions in this case. Gordon et.al.²⁵ measured the angular distributions of fission fragments in the $^{12}\text{C} + ^{197}\text{Au}$ system at different incident projectile energies. They concluded that the average excitation energy of the fissioning nuclei is independent of projectile energy. At high excitation, fast

processes like particle emission dominate; the slower fission process cannot compete until the excitation energy has been decreased to about 25 MeV. We do not consider the possibility of "fast fission" processes since, in the reaction of 20 MeV/A ^{12}C with ^{197}Au , the critical angular momentum of fusion is 20 \hbar smaller than the value of the angular momentum at which the fission barrier of the compound nucleus vanishes²⁴.

The determination of isomer ratios gives a rough measure of the energy and angular momentum in the precursor nuclides. The isomer ratios measured in this work are tabulated in Table 2, together with the isomer ratios for the same nuclides determined in other reactions²⁹⁻³⁴. The isomer ratios of ^{116}Sn and ^{119}Te in the present work are very nearly equal to those obtained from the complete fusion reactions $^{115}\text{In}(\alpha, 3n)$ and $^{118}\text{Sn}(\alpha, 3n)$ at $E_\alpha = 33 \text{ MeV}$ ³¹. The isomer ratio we have determined for ^{121}Te is only somewhat larger than that from $^{120}\text{Sn}(\alpha, 3n)$ at $E_\alpha = 33 \text{ MeV}$ ³¹. Ref. 31 gives an isomer ratio for ^{126}Sb from the $^{124}\text{Sn}(\alpha, pn)$ reaction at $E_\alpha = 36.5 \text{ MeV}$ which is similar to the $(\alpha, 3n)$ values given above. However, the isomer ratio of ^{126}Sb produced in the reaction of 94 MeV ^{12}C with ^{209}Bi ³⁵, which proceeds largely via a complete fusion mechanism, is about 2.5 times larger than that from the $^{124}\text{Sn}(\alpha, pn)$ reaction. The small values of the isomer ratios for the fission products obtained in our experiments is another indication that much of the fission cross section arises from low angular momentum sequential fission processes rather than from the high angular momentum complete fusion process.

B. Target-like products

The cross sections of target-like reaction products are plotted in figure 1 with the cross sections of the fission

products. As shown in figure 3, the charge dispersions of $A = 200$ to $A = 204$ can be fit with single Gaussian distributions with width parameters ($2\sigma^2$) of about 1.6. For $A = 196$ to $A = 199$, the charge dispersions seem to have two components. The high- Z nuclides can be described with a width parameter of 1.1, while the low- Z peaks are much narrower, with $2\sigma^2 = 0.6$. The most probable charge associated with the small width parameter increases with mass number, consistent with a quasi-elastic reaction mechanism where the reactions are centered about the (Z,A) of the target. The more neutron deficient products described with the larger width parameter are due to some combination of complete fusion, deep-inelastic and/or several-nucleon-transfer processes. The most probable charge of these products remains constant at $Z = 82$ for nuclei with $A = 198$ to $A = 202$. This is due, in part, to the effect of the $Z = 82$ shell on the transfer process and on its effect on the fission survival probability of the primary reaction products.

The ALICE calculation described earlier did not reproduce the cross sections of most of the target-like products. The systematic behavior of the calculated cross sections was contrary to that observed in the experiment, with cross sections falling off from the compound nucleus (Z,A) . The experimental cross sections of the Tl, Pb and Bi isotopes are one to two orders of magnitude larger than the calculated cross sections. The calculation did reproduce the cross sections of the polonium isotopes, except for ^{202}Po and ^{204}Po . This, and the sudden shift of the charge distributions away from $Z_p = 82$ for $A = 203$ and $A = 204$ we attribute to the de-excitation of primary products near the (Z,A) of the compound nucleus by the emission of non-equilibrium high energy nucleons.

In figure 4, the cross sections of the Tl, Pb, Bi and Po isotopes are plotted vs. the Q_{gg} for their formation via a "compound nucleus". Volkov³⁶ has used the Q_{gg} method to extract the nuclear temperature of partial fusion reactions from projectile-like reaction products, assuming a binary reaction mechanism. Jacmart et.al.³⁷ were not able to reproduce a similar systematic Q_{gg} dependence. Here, the ^{12}C projectile is so small that we assume that the complementary fragment for the production of species at a significantly higher Z than the target nucleus exists as a set of discrete, unbound nucleons. We have, in effect, assumed for the purpose of the Q_{gg} calculation that the polonium isotopes are produced in $^{197}\text{Au}(^{12}\text{C}, \text{pxn})$ reactions, that the bismuth isotopes are produced in $^{197}\text{Au}(^{12}\text{C}, 2\text{pxn})$ reactions, etc. Since the binding energy of the neutron is positive for all the target-like products, the mass numbers of the isotopes of a given element decrease from left to right in figure 4. The solid lines are drawn parallel to the linear fit to the bismuth data. The strongest deviations from linear behavior occur in the thallium isotopes, where the size of the complementary fragments (^4Be) for the more neutron deficient products makes the discrete-nucleon assumption untenable. Since we are plotting evaporation residue cross sections rather than the cross sections of primary products, the slope no longer directly relates to the reaction temperature; in fact, the slope is of the opposite sign from that obtained by Volkov³⁶.

The charge corrected mass distribution of target-like products is shown in figure 1b along with that of the fission products. In the case of $A = 196$ to $A = 199$, the quasi-elastic component (closed circles) and the deep-inelastic component (triangles) were integrated separately, then summed to give

the data plotted as open circles. The total cross section for the production of target-like products ($A = 170$ to 204) is about 1700 mb. Combined with the fission cross section of 1700 mb, this gives a total reaction cross section of about 3.4 b, in agreement with the value calculated by Wilcke et.al.²⁴ of 3.3 b.

The isotopic distributions for $Z = 78$ to $Z = 84$ are plotted in figure 5. In general, there is a downward trend in the product cross sections as the mass and charge of the products increase from the target (Z, A). The apparent exception for the mercury isotopes ($Z+1$) is due to the fact that most of the observed cross sections were for only one half of an isomer pair. The cross sections of the thallium ($Z+2$) and bismuth ($Z+4$) isotopes are much lower than those arising from the $^{12}\text{C} + ^{197}\text{Au}$ reaction at lower projectile energies³⁸.

The isomeric yield ratios of target-like products are tabulated in Table 2. Due to the angular momentum dependence of the competition of fission to particle evaporation, the obtained isomer ratios do not directly relate to the angular momentum of the composite system or the spin distribution in the primary reaction products. They do give some indication of the reaction mechanism resulting in these evaporation residues. The cross section ratio of high spin to low spin isomers in ^{198}Tl , ^{196}Tl and ^{197}Hg are all larger than those for the typical quasi-elastic products ^{196}Au and ^{198}Au . Even at these projectile energies, the "thermalization" of angular momentum in the quasi-elastic channels is very small, on the order of that introduced by 13 MeV neutrons in the $^{197}\text{Au}(n,2n)$ reaction. The relative sizes of the ^{198}Tl and ^{196}Tl isomer ratios we cannot explain.

IV. Conclusion

The cross sections of about 250 nuclides were obtained in the reaction of 20 MeV/A ^{12}C with ^{197}Au .

The charge dispersion of fission products had a Gaussian shape with a width parameter ($2\sigma^2$) of 1.6, which is larger than those obtained from lower energy systems. The FWHM of the mass yield curve of the fission products was 38 mass units, and the fission cross section was about 1.7 b. Both these values are larger than those obtained in low energy heavy ion induced fission. The broadening of the charge dispersion and mass distribution of the fission products may be attributed to the large variety of fissioning nuclei of high angular momentum. The isomer ratios of the fission products were similar to those measured in low energy systems.

The charge dispersions of $A = 196$ to $A = 199$ have two components, one corresponding to quasi-elastic processes, and the other corresponding to deep-inelastic and/or complete fusion processes. The cross sections of higher Z elements were smaller than those of lower Z elements in the trans-target element region, contrary to the result expected from an evaporation calculation. The summed cross section of target-like products was about 1.7 b. The total reaction cross section was about 3.4 b, which is in agreement with the theoretical estimate of 3.3 b.

Acknowledgement

The authors would like to thank the staff and crew of the 88-inch Cyclotron for their assistance and support. We would also like to thank / ^{Professor} W. Loveland for his interest and Dr. Y. Morita for his help with irradiations. One of us (H.K.) would like to thank the Lawrence Berkeley Laboratory for a pleasant

stay and is indebted to the members of the LBL-INS collaboration group. The continuous encouragement of Prof. H. Nakahara is gratefully acknowledged.

Acknowledgement: This work was supported by the Director, Office of Energy Research Division of Nuclear Physics of the Office of High Energy and Nuclear Physics of the U.S. Department of Energy under Contract No. DE-AC03-76SF00098.

Appendix

The following are notes on the chemical procedures used to separate the elements near gold from the fission products and from each other.

Hafnium: After separation from the lanthanides, hafnium was co-precipitated with barium fluorozirconate. The precipitate was dissolved in boric acid and nitric acid, and a hydroxide precipitation was performed by adding ammonium hydroxide. The precipitate was dissolved in a small amount of hydrochloric acid, and loaded on an anion exchange column (Dowex AG 1-X8). Hafnium was eluted with a 4N HCl-0.1N HF solution.

Tantalum: Tantalum oxide was precipitated from fuming HNO_3 . The precipitate was washed with NH_4OH to remove tungsten (see below), and then tantalum was dissolved in hydrofluoric acid. Lanthanum hydroxide, antimony sulfide and barium fluorozirconate scavenge procedures were performed. Tantalum oxide was re-precipitated by adding boric acid in a nitric acid solution.

Tungsten: Tungsten was precipitated from fuming HNO_3 . After dissolving in NH_4OH and scavenging with $\text{Fe}(\text{OH})_3$, tungsten was precipitated with 8-hydroxyquinoline in an ammonium acetate-acetic acid buffer solution.

Rhenium: Rhenium was distilled from concentrated H_2SO_4 into a NaOH solution. After scavenging with $\text{Fe}(\text{OH})_3$ and $\text{Ru}(\text{OH})_3$ precipitations, rhenium was precipitated with tetraphenyl arsonium. In this work, however, we could not measure the gamma-rays of any rhenium isotopes, probably due to their small cross sections and the low chemical yield of this procedure.

Osmium: Osmium was distilled from concentrated HNO_3 into 6N NaOH, and precipitated with hydrogen sulfide with the addition of hydrochloric acid.

Iridium: After separation from platinum with an ethyl acetate extraction, iridium was reduced to the metallic state with formic acid.

Platinum: Initially gold and thallium contaminants were extracted from a 3N HCl solution with ethyl acetate (see below). Then platinum(IV) was reduced to platinum(II) with Sn^{2+} , followed by a silver chloride scavenge. Platinum(II) was extracted into ethyl acetate. After evaporating the organic phase, platinum was reduced to the metallic state with magnesium powder in 2N HCl.

Gold: Gold was extracted from 6N HCl solution into ethyl acetate. The organic layer was transferred to a beaker containing hydrazine hydrochloride solution, evaporated, and the metallic gold precipitate was filtered.

Mercury: Mercury was precipitated with hydrogen sulfide from 0.3N HCl solution, dissolved with a sodium sulfide-sodium hydroxide solution, and reprecipitated with ammonium chloride. After dissolving the precipitate in concentrated HCl and KI solution, mercury was precipitated with hydrogen sulfide.

Thallium: Thallium was extracted into ethyl acetate from a 6N HCl solution. After separation from gold (see above), thallium was precipitated with sodium iodide.

Lead: Lead sulfide was precipitated from 0.3N HCl solution. After washing with 6N HCl, the lead sulfide was dissolved in concentrated HCl. Finally, lead was precipitated with sodium chromate from an ammonium acetate buffer solution.

Bismuth: A bismuth sulfide precipitation was performed from a 0.3N HCl solution, then dissolved in 6N HCl. Then a silver chloride scavenge was applied. Finally, precipitation of BiOCl was obtained by digesting a dilute hydrochloric acid solution.

Polonium: (for gamma-ray counting) Gold and thallium were extracted into ethyl acetate from 3N HCl solution. Polonium was extracted from a potassium iodide-hydrochloric acid mixture with ethyl acetate. After back-extraction with 3N HCl, polonium self-deposited onto a silver foil from a 0.5N HCl solution containing hydrazine-hydrochloride.

(for alpha counting) The chemical yield of polonium in volatilization experiments to produce alpha sources was determined by the direct comparison of the ^{204}Po gamma-ray activity after the end of the alpha particle measurements with that obtained in the chemistry described above, where ^{210}Po was used as a tracer. With this method, however, the statistical error was large due to poor counting statistics. Five test runs were made with the volatilization apparatus using a known amount of ^{210}Po evaporated on an aluminum foil. The chemical yield was fairly constant, being (83 +- 4)%. This chemical yield was independent of whether the polonium source was placed with the activity side up or down, which means the evaporation yield is roughly independent of source depth. The reproducible chemical yield from the test runs was applied to the experimental runs, and gave answers in each case which were consistent with the ^{204}Po measurements.

References

1. W. Loveland, R. J. Otto, D. J. Morrissey, and G. T. Seaborg, Phys.Rev.Lett. 39, 320 (1977).
2. W. Loveland, R. J. Otto, D. J. Morrissey, and G. T. Seaborg, Phys.Lett. 69B, 284 (1977).
3. C. R. Rudy and N. T. Porile, Phys.Lett. 59B, 240 (1975).
4. J. B. Cumming, R. W. Stoenner, and P. E. Haustein, Phys.Rev. C14, 1554 (1976).
5. D. J. Morrissey, W. Loveland, M. de Saint Simon, and G. T. Seaborg, Phys.Rev. C21, 1783 (1980).
6. S. B. Kaufman, E. P. Steinberg, B. D. Wilkins, and D. J. Henderson, Phys.Rev. C22, 1897 (1980).
7. C. K. Gelbke, Nucl.Phys. A387, 79c (1982), and Refs. therein.
8. T. C. Awes, S. Saini, G. Poggi, C. K. Gelbke, and D. Cha, Phys.Rev. C25, 2361 (1982).
9. R. Glasow, G. Gaul, B. Ludewigt, R. Santo, H. Ho, W. Kuhn, U. Lynen, and W. F. J. Muller, Phys.Lett. 120B, 71 (1983).
10. M. Blann, Phys.Rev. C23, 205 (1981).
11. T. J. M. Symons, P. Doll, M. Bini, D. L. Hendrie, J. Mahoney, G. Mantzouranis, D. K. Scott, K. Van Bibber, Y. P. Viyogi, H. H. Wieman, and C. K. Gelbke, Phys.Lett. 94B, 131 (1980).
12. Ch. Egelhaaf, M. Bürgel, H. Fuchs, A. Gamp, H. Homeyer, D. Kovar, and W. Rauch, Nucl.Phys. A405, 397 (1983).
13. J. Kleinberg, Los Alamos Scientific Laboratory, Report No. LA-1721 (1967).
14. D. J. Morrissey, D. Lee, R. J. Otto, and G. T. Seaborg, Nucl.Inst.Meth. 158, 499 (1979).
15. I. Binder, R. Kraus, R. Klein, D. Lee, and M. M. Fowler, Lawrence Berkeley Laboratory, Report LBL-6515, UC-34c (1977).

16. C. M. Lederer and V. S. Shirley, "Table of Isotopes", 7th ed. New York: John Wiley and Sons, 1978.
17. U. Reus, W. Westmeier and I. Warnecke, "Gamma-Ray Catalog", Gesellschaft für Schwerionenforschung, Report 79-2 (1979).
18. M. Blann, Phys.Rev. 123, 1356 (1961).
19. A. C. Wahl, Proc. IAEA Symp. Phys. Chem. Fission, Salzburg, Vol. I, p. 317. Vienna: IAEA, 1965.
20. J. A. McHugh and M. C. Michel, Phys.Rev. 172, 1160 (1968).
21. C. Cabot, C. Ngo, J. Peter, and B. Tamain, Nucl.Phys. A244, 134 (1975).
22. J. G. Cuninghame, J. A. B. Goodall, J. E. Freeman, G. W. A. Newton, V. J. Robinson, J. L. Durell, G. S. Foote, I. S. Grant, and J. D. Hemingway, Proc. 4th Symp. Phys. Chem. Fission, IAEA-SM-241/D2, p. 551 (1979).
23. B. Borderie, M. Berlinger, D. Gardes, F. Hanappe, L. Nowicki, J. Peter, B. Tamain, S. Agarwal, J. Girard, C. Gregoire, J. Matuszek, and C. Ngo, Z.Phys. A299, 263 (1981).
24. W. W. Wilcke, J. R. Birkelund, H. J. Wollersheim, A. D. Hoover, J. R. Huizenga, W. U. Schröder, and L. E. Tubbs, At.Nucl.Data Tables 25, 389 (1980).
25. G. E. Gordon, A. E. Larsh, T. Sikkeland, and G. T. Seaborg, Phys.Rev. 120, 1341 (1960).
26. H. C. Britt and A. R. Quinton, Phys.Rev. 120, 1768 (1960).
27. A. Khodai-Joopari, Lawrence Berkeley Laboratory, Report UCRL-16486 (1969).
28. F. Plasil, Oak Ridge National Laboratory, Report TM-6054 (1977).
29. H. S. Hans, M. L. Sehgel, and P. S. Gill, Nucl.Phys. 20, 183 (1960).
30. V. M. Alazov, M. Milanov, D. Kolev, N. Nenoff, and B. Todorov, Z.Phys. A296, 65 (1980).

31. I. S. Grant and M. Rathle, *J.Phys.G* 5, 1741 (1979).
32. R. J. Prestwood and B. P. Bayhurst, *Phys.Rev.* 121, 1438 (1961).
33. R. Vandenbosch and J. R. Huizenga, *Phys.Rev.* 120, 1313 (1960).
34. Y. Nagame, H. Nakahara, and Y. Murakami, *Intern.J.Applied Radiation and Isotopes* 30, 669 (1979).
35. J. G. Cuninghame, J. A. B. Goodall, J. E. Freeman, G. W. A. Newton, V. J. Robinson, J. L. Durell, G. S. Foote, I. S. Grant, and M. Rathle, *J.Phys.G* 6, 127 (1980).
36. V. V. Volkov, *Proc.Symp. on Classical and Quantum Mechanical Aspects of Heavy Ion Collisions*, Heidelberg, 1975.
37. J. C. Jacmart, P. Colombani, H. Doubre, N. Frascaria, N. Poffe, M. Riou, J. C. Roynette, C. Stephan, and A. Weidinger, *Nucl.Phys.* A242, 175 (1975).
38. R. Bimbot, D. Gardes, and M. F. Rivet, *Nucl.Phys.* A189, 193 (1972).

TABLE I. Cross sections measured in 20 MeV/A $^{12}\text{C} + ^{197}\text{Au}$.

Nuclide	Cross section(mb)	Type ^a	Method ^b	Half life	E_{γ} (keV)	I_{γ} (%)	Ref
^{71}As	.336 +.053	CD	C	2.7 d	174.9	74.	15
^{72}As	1.21 +.19	I	C,D	1.083 d	834.0	69.5	15
^{74}As	8.49 +1.24	I	C,D	17.70 d	595.9	59.2	15
^{76}As	14.7 +2.1	I	C,D	1.096 d	559.1	44.6	15
^{77}As	18.6 +3.2	CR	C	1.613 d	239.1	1.4	15
^{78}As	17.6 +3.6	CR	C,D	1.510 h	613.7	31.	15
^{73}Se	.288 +.060	CD	C	7.18 h	360.9	97.	16
^{75}Se	5.08 +.22	CD	C	118.45 d	264.65	58.	16
$^{81}\text{Se}^{\text{m}}$	21.1 +15.6	CR	C	57.28 m	102.7	9.7	16
^{82}Br	23.9 +6.7	I	D	1.479 d	698.2	27.9	15
$^{84}\text{Br}^{\text{m}}$	7.46 +1.13	CR	D	6. m	1462.8	97.	16
$^{85}\text{Kr}^{\text{m}}$	2.99 +1.35	CR	D	4.481 h	151.3	76.1	15
^{88}Kr	12.6 +8.3	CR	D	2.86 h	196.3	26.3	16
$^{82}\text{Rb}^{\text{m}}$	2.90 +2.40	I	D	6.2 h	618.9	37.17	16
$^{84}\text{Rb}^{\text{m}}$	12.8 +4.1	I	D	20.405 m	247.9	65.	15
$^{84}\text{Rb}^{\text{g}}$	2.92 +1.70	I	C	32.77 d	881.6	74.	16
^{86}Rb	4.66 +1.74	I	C	18.82 d	1077.2	8.79	16
^{83}Sr	1.31 +.34	CD	C	1.35 d	762.5	29.4	15
$^{85}\text{Sr}^{\text{m}}$.463 +.148	I	C	68. m	231.7	84.5	16
$^{85}\text{Sr}^{\text{g}}$	13.1 +1.1	I	C	64.85 d	514.	100.	16
^{91}Sr	12.9 +3.4	CR	C	9.5 h	1024.3	33.4	16
^{92}Sr	5.07 +.56	CR	C,D	2.71 h	1383.9	90.	15
^{93}Sr	.764 +.181	CR	C	7.43 m	590.18	73.	16
$^{85}\text{Y}^{\text{m}}$.688 +.100	CD	C	4.7 h	231.7	13.	16
$^{85}\text{Y}^{\text{g}}$.109 +.023	CD	C	2.68 h	504.5	64.	16
$^{86}\text{Y}^{\text{m}}$	2.13 +1.72	I	C,D	48. m	208.2	94.	16
$^{86}\text{Y}^{\text{g}}$	3.25 +.16	I	C,D	14.74 h	627.72	32.6	16
$^{87}\text{Y}^{\text{m}}$	11.3 +2.0	CD	C,D	13.2 h	381.1	78.	16
$^{87}\text{Y}^{\text{g}}$	13.6 +2.8	I	D	80.3 h	484.8	92.	16
^{88}Y	26.3 +.8	I	C	106. d	898.0	92.	15
$^{90}\text{Y}^{\text{m}}$	35.7 +6.4	I	C	3.19 h	202.4	97.	15
$^{91}\text{Y}^{\text{m}}$	32.5 +2.5	I	D	49.694 m	555.6	94.9	15
^{92}Y	20.6 +6.9	CR	C,D	3.530 h	934.5	13.7	15
^{93}Y	16.3 +2.8	CR	C	10.2 h	267.	6.8	16
^{94}Y	6.71 +1.08	CR	C	18.7 m	918.8	56.	16
^{95}Y	2.65 +.48	CR	C	10.3 m	954.2	19.	16
^{86}Zr	.438 +.104	CD	C	16.5 h	243.0	96.	15
^{87}Zr	.280 +.263	CD	C	1.57 h	1228.	4.	16
^{88}Zr	3.19 +.18	CD	C,D	85. d	392.8	97.	15
^{89}Zr	10.5 +1.6	CD	C	3.271 d	909.2	100.	15
^{95}Zr	25.3 +6.6	CR	C	64. d	756.7	54.6	16
^{97}Zr	4.73 +.12	CR	C	16.9 h	743.4	92.8	16
^{90}Nb	3.50 +.76	CD	C	14.6 h	1129.2	92.66	16
$^{92}\text{Nb}^{\text{m}}$	19.7 +18.4	I	C,D	10.1 d	934.5	99.1	15
$^{95}\text{Nb}^{\text{g}}$	46.8 +2.5	I	C,D	35.1 d	765.8	99.	15
^{96}Nb	35.6 +10.2	I	D	23.501 h	1091.3	49.4	15
^{97}Nb	28.0 +.04	I	C,D	73.62 m	658.1	99.	15
$^{98}\text{Nb}^{\text{m}}$	8.23 +1.69	CR	D	51.005 m	787.2	95.	15
$^{93}\text{Mo}^{\text{m}}$	3.13 +.09	CD	C	6.95 h	1477.2	99.1	16
^{99}Mo	33.2 +2.7	CR	D	66.02 h	739.6	14.	16
^{102}Mo	3.35 +1.45	CR	D	11.0 m	475.0	59.	15
^{94}Tc	.623 +.351	CD	C	293. m	871.01	100.	16
^{95}Tc	3.32 +.77	CD	C	20. h	765.8	94.	15

TABLE I. continued.

Nuclide	Cross section(mb)	Type ^a	Method ^b	Half life	E _γ (keV)	I _γ (%)	Ref
⁹⁶ Tc	6.71 ±1.60	I	C,D	4.3 d	849.9	97.8	15
⁹⁹ Tc ^m	6.96 ±.14	I	D	6.02 h	140.5	89.	16
¹⁰¹ Tc	10.2 ±1.6	I	D	14.00 m	306.8	88.7	15
¹⁰² Tc ^m	15.4 ±.8	I	D	4.35 m	474.8	85.0	16
¹⁰⁴ Tc	4.95 ±.18	CR	D	18.00 m	357.8	84.4	15
⁹⁷ Ru	1.61 ±.14	CD	C,D	2.89 d	215.7	87.6	15
¹⁰³ Ru	51.0 ±1.1	CR	C,D	39.6 d	497.1	90.	15
¹⁰⁵ Ru	17.8 ±.3	CR	C,D	4.44 h	469.4	17.5	15
¹⁰⁰ Rh	2.30 ±.13	I	C	20.8 h	539.6	78.4	16
¹⁰¹ Rh ^m	5.03 ±.21	CD	C,D	4.34 d	306.8	100.	15
¹⁰⁵ Rh	28.3 ±1.9	I	C	35.47 h	318.9	19.	16
¹⁰⁶ Rh ^m	14.1 ±.4	I	C,D	130. m	717.2	19.2	16
¹⁰⁸ Rh ^B	7.04 ±3.33	CR	D	5.9 m	434.2	100.	15
¹⁰⁰ Pd	.123 ±.009	CD	C	3.63 d	539.6 ^f	78.4	16
¹⁰¹ Pd	.510 ±.043	CD	C	8.47 h	296.29	18.	16
¹⁰⁹ Pd	25.5 ±.5	CR	C	13.427 h	88.04	3.6	16
¹¹¹ Pd ^m	2.87 ±.70	CR	C	5.5 h	172.2	32.33	16
¹¹² Pd	2.10 ±.03	CR	C	21.12 h	617.4 ^f	42.	16
¹⁰³ Ag	.376 ±.124	CD	C	1.095 h	118.7	22.2	15
¹⁰⁴ Ag ^m	.600 ±.393	I	C	33.5 m	767.6 ^f	65.78	16
¹⁰⁴ Ag ^g	<.51 ^c	I	C	69.2 m	767.6	65.78	16
¹⁰⁵ Ag	4.21 ±.15	CD	C	41.0 d	344.4	42.	15
¹⁰⁶ Ag ^m	6.43 ±.08	I	C	8.410 d	1045.7	29.7	15
¹¹⁰ Ag ^m	23.7 ±.6	I	C	253. d	657.7	93.8	15
¹¹¹ Ag	36.2 ±3.8	I ^d	C	7.47 d	342.1	4.6	15
¹¹² Ag	13.8 ±.4	I	C	3.14 h	617.4	42.	16
¹¹³ Ag	12.8 ±.4	CR	C	5.299 h	298.4	8.2	15
¹⁰⁷ Cd	1.53 ±.55	CD	C	6.499 h	93.1	4.6	15
¹¹¹ Cd ^m	18.1 ±1.2	I	C,D	46.8 m	245.4	94.	15
¹¹⁵ Cd ^g	1.42 ±.48	CR	C	2.221 d	527.9	27.5	15
¹⁰⁹ In	1.16 ±.41	CD	C	4.301 h	203.5	72.1	15
¹¹⁰ In ^m	2.64 ±.59	I	C,D	4.901 h	844.7	94.9	15
¹¹¹ In	6.85 ±2.38	CD	C	2.83 d	171.3	90.3	15
¹¹⁴ In ^m	15.5 ±5.5	I	C	49.5 d	558.3	4.7	15
¹¹⁶ In ^m	13.8 ±4.8	I	C,D	54.101 m	1293.4	85.	15
¹¹⁵ Sb	5.64 ±1.06	CD	C	31.8 m	498.	99.1	16
¹¹⁶ Sb ^m	4.26 ±.86	I	C,D	1.005 h	972.6	72.	15
¹¹⁶ Sb ^g	3.13 ±.99	I	D	15.998 m	1293.7	88.	15
¹¹⁸ Sb ^m	9.87 ±.43	I	C,D	5.1 h	253.5	99.	16
¹²⁰ Sb ^m	<.69 ^c	I	C	5.8 h	1023.1	99.	15
¹²⁰ Sb ^B	6.66 ±.42	I	C,D	5.76 d	1171.7	100.	16
¹²² Sb	4.73 ±.38	I	C	2.681 d	564.1	70.	16
¹¹⁶ Te	1.27 ±.11	CD	C,D	2.50 h	94.1	29.	16
¹¹⁷ Te	<.19 ^c	CD	C	61. m	719.7	65.	16
¹¹⁸ Te	7.99 ±2.49	I	C	6.0 d	1229.5 ^f	2.5	16
¹¹⁹ Te ^m	5.83 ±.38	I	C	4.68 d	153.5	66.	16
¹¹⁹ Te	1.93 ±.17	I	C	16.05 h	644.01	84.	16
¹²¹ Te ^m	10.5 ±1.4	I	C	154. d	212.2	83.	16
¹²¹ Te ^g	1.83 ±.39	I	C,D	16.78 d	573.01	80.3	16
¹²³ Te ^m	6.51 ±.25	I	C	119.7 d	159.	83.6	16
¹¹⁸ I	1.79 ±.48	CD	C	14.3 m	605.2	95.	16
¹¹⁹ I	.568 ±.242	CD	C	19.296 m	257.6	95.	15
¹²⁰ I ^m	.6.1 ±.153	I	C	53. m	560.4	100.	16

TABLE I. continued.

Nuclide	Cross section(mb)	Type ^a	Method ^b	Half life	E _γ (keV)	I _γ (%)	Ref
120 _{Ig}	1.05 ±.23	CD	C	1.35 h	560.4	73.	16
121 _I	4.14 ±.29	CD	C,D	2.12 h	212.5	84.3	15
123 _I	9.31 ±.77	CD	C,D	13.099 h	159.1	83.	15
124 _I	6.39 ±.78	I	C	4.17 d	602.7	62.	15
126 _I	3.37 ±.75	I	C	13.0 d	388.6	34.9	15
130 _I	.542 ±.117	I	C	12.36 h	668.4	94.	16
127 _{Xe}	14.2 ±1.9	CD	D	36.4 d	202.8	60.8	15
129 _{Cs}	4.64 ±.65	CD	C	33.35 h	371.9	32.	16
132 _{Cs}	.683 ±.083	I	C	6.474 d	667.5	97.5	16
126 _{Ba}	2.55 ±.50	CD	C	100. m	388.6 ^f	42.	16
128 _{Ba}	1.61 ±.45	CD	C	2.43 d	443. ^f	25.8	16
131 _{Ba^m}	2.19 ±2.04	I	C,D	14.60 m	107.	56.	16
131 _{Ba^g}	4.90 ±.95	CD	C,D	12.0 d	123.7	28.	16
133 _{Ba^m}	1.08 ±.34	I	C	38.9 h	275.6	17.5	16
130 _{La}	.797 ±.465	I	C	8.7 m	357.3	81.	16
131 _{La}	1.81 ±.97	CD	C	61. m	108.1	24.	16
132 _{La^m}	4.60 ±3.10	I	D	24.307 m	135.8	43.0	16
132 _{La^g}	2.02 ±.54	I	C	4.8 h	464.55	76.	16
134 _{La}	4.42 ±1.95	I	C	6.67 m	604.7	5.04	16
136 _{La}	4.83 ±2.23	I	C	9.87 m	818.51	2.6	16
130 _{Ce}	.163 ±.157	CD	C	25. m	357.3 ^f	81.	16
131 _{Ce}	2.90 ±.92	CD	C	10.5 m	169.6	20.	16
132 _{Ce}	.824 ±.160	CD	C	3.51 h	464.55 ^f	76.	16
133 _{Ce}	.479 ±.086	CD	C	5.4 h	130.7	42.0	15
134 _{Ce}	1.59 ±1.19	CD	C	75.9 h	604.7 ^f	5.04	16
135 _{Ce}	3.03 ±.55	CD	C	17.6 h	265.3	46.	15
137 _{Ce^m}	1.29 ±.05	I	C	34.4 h	254.3	11.1	16
137 _{Ce^g}	2.92 ±.96	CD	C	9.0 h	447.15	2.2	16
139 _{Ce}	3.16 ±.57	CD	C	137.2 d	165.9	80.	16
141 _{Ce}	.038 ±.011	CR	C	32.55 d	145.4	49.3	16
136 _{Pr}	.927 ±.146	I	C	13.1 m	539.8	52.44	16
138 _{Pr^m}	1.44 ±.43	I	C	2.02 h	789.0	100.	16
136 _{Nd}	.451 ±.114	CD	C	50.65 m	547.9	12.	16
137 _{Nd}	.571 ±.141	CD	C	38.5 m	580.6	13.	16
138 _{Nd}	2.02 ±1.20	CD	C	5.04 h	326.3	2.9	16
139 _{Nd^m}	.872 ±.045	I	C	5.5 h	113.9	39.55	16
140 _{Pm^m}	.269 ±.125	I	C	5.95 m	419.9	91.63	16
141 _{Pm}	2.53 ±.94	CD	C	20.9 m	1223.26	4.	16
144 _{Pm}	.803 ±.665	I	C	349. d	696.5	100.	16
141 _{Sm^m}	.300 ±.090	CD	C	10.2 m	403.9	42.4	16
141 _{Sm^g}	.192 ±.054	CD	C	22.5 m	196.6	73.6	16
142 _{Sm}	.269 ±.114	CD	C	72.49 m	1576. ^f	3.0	16
145 _{Eu}	.398 ±.071	CD	C	5.93 d	893.5	65.	16
146 _{Eu}	.429 ±.102	I	C	4.7 d	747.2	97.8	15
147 _{Eu}	.770 ±.173	I	C	24.3 d	197.3	23.	15
148 _{Eu}	.286 ±.001	I	C	54. d	550.2	99.	16
145 _{Gd}	.200 ±.070	CD	C	21.8 m	1757.8	35.	16
146 _{Gd}	.079 ±.025	CD	C	48.3 d	115.3	45.	15
147 _{Gd}	.286 ±.068	CD	C	1.458 d	229.3	57.0	15
149 _{Gd}	.429 ±.021	CD	C	9.25 d	149.7	53.37	16
147 _{Tb}	.123 ±.049	CD	C	1.61 h	1153.	75.	16
151 _{Tb}	.329 ±.157	CD	C	17.6 h	108.1	25.22	16
152 _{Tb}	.234 ±.021	I	C	17.5 h	344.3	66.	16

TABLE I. continued.

Nuclide	Cross section(mb)	Type ^a	Method ^b	Half life	E _γ (keV)	I _γ (%)	Ref
153Tb	.411 ±.027	I	C	2.30 d	211.94	40.	16
155Tb	.376 ±.066	CD	C	5.32 d	105.3	23.	16
156Tb	.049 ±.010	I	C	5.35 d	534.3	67.0	16
152Dy	.215 ±.040	CD	C	2.37 h	257.	97.6	16
153Dy	.877 ±.099	CD	C	6.29 h	254.23	5.0	16
155Dy	.332 ±.063	CD	C	10. h	227.	68.	16
157Dy	.337 ±.063	CD	C	8.1 h	326.3	95.0	15
156Ho	.460 ±.070	CD	C	54.994 m	266.4	72.3	15
160Er	.126 ±.050	CD	C	1.225 d	728.1 ^f	61.	15
161Er	.225 ±.045	CD	C	3.24 h	826.5	61.	16
167Tm	.114 ±.087	CD	C	9.25 d	207.8	41.0	16
166Yb	.224 ±.127	CD	C	56.7 h	184.3 ^f	15.9	16
167Yb	.086 ±.073	I	C	17.7 m	113.32	54.	16
169Lu	.118 ±.049	CD	C	34.06 h	191.2	21.55	16
170Hf	<.05 ^c	CD	C	15.92 h	164.78	33.	16
173Hf	.110 ±.007	I	C	24.0 h	123.69	83.	16
173Ta	.064 ±.004	CD	C	3.701 h	123.69 ^f	83.	16
174Ta	.057 ±.057	CD	C	1.2 h	206.5	66.2	15
175Ta	.164 ±.017	CD	C	10.5 h	207.4	13.3	15
176Ta	.197 ±.028	CD	C	8.1 h	1159.3	24.0	15
177Ta	.192 ±.025	CD	C	2.358 d	113.0	6.0	15
178Ta	.014 ±.005	I	C	2.45 h	325.6	94.1	16
176W	.150 ±.010	CD	C	2.3 h	100.2	71.	15
177W	.141 ±.013	CD	C	2.25 h	115.7	43.0	15
178W	.680 ±.623	CD	C	21.5 d	1350.6 ^f	1.17	16
180Os	.331 ±.103	CD	C	21.7 m	902.4 ^f	98.	16
181Os _g	.107 ±.008	CD	C	105. m	238.7	46.2	16
182Os	1.12 ±.08	CD	C	22.10 h	180.2	33.152	16
183Os _m	.864 ±.044	CD	C	9.9 h	1102.	55.	16
183Os _g	.625 ±.039	CD	C	13. h	114.4	19.8	16
185Os	1.37 ±.19	CD	C	93.6 d	646.07	81.	16
184Ir	<3.5 ^c	CD	D	3.101 h	119.8	33.2	15
186Ir _m	<4.4 ^c	I	D	1.75 h	630.3	19.3	15
188Ir	6.83 ±1.22	I	C	1.729 d	633.1	22.	15
186Pt	2.15 ±.07	CD	C	2.0 h	434.8 ^f	33.7	16
187Pt	5.17 ±.27	CD	C	2.35 h	201.5	7.6	15
188Pt	19.0 ±.5	CD	C	10.2 d	187.6	19.2	16
189Pt	34.5 ±.6	CD	C,D	10.87 h	243.5	4.4	16
191Pt	9.03 ±.22	I	C	3.0 d	409.4	7.9	15
197Pt	1.88 ±.11	CR	C	18.3 h	191.4	3.485	16
189Au	11.1 ±2.7	CD	C	28.7 m	721.4 ^f	5.8	16
190Au	11.7 ±1.0	I	C	42.8 m	296.0	71.	16
191Au	11.1 ±.6	I	C	3.199 h	586.4	19.2	15
192Au	7.97 ±.76	I	C	5.03 h	316.6	89.4	15
193Au	10.5 ±1.8	I ^e	C	17.5 h	255.6	7.	16
194Au	32.9 ±2.5	I	C,D	39.5 h	328.47	61.	16
196Au _m	5.80 ±.38	I	C,D	9.701 h	147.7	42.0	15
196Au _g	139. ±7.	I	C,D	6.18 d	355.7	88.0	15
198Au _m	1.23 ±.14	I	C	2.27 d	214.9	78.7	15
198Au _g	17.9 ±.9	I	C	2.69 d	411.8	94.7	15
199Au	.794 ±.122	CR	C	3.148 d	158.24	39.	16
190Hg	19.6 ±.8	CD	D	20.002 m	142.7	96.0	15
191Hg	26.7 ±1.5	CD	C	50.8 m	252.6	55.1	15

TABLE I. continued.

Nuclide	Cross section(mb)	Type ^a	Method ^b	Half life	E _γ (keV)	I _γ (%)	Ref
¹⁹² Hg	23.5 ±4.7	I	C	4.901 h	274.8	46.1	15
¹⁹³ Hg ^m	23.1 ±1.1	I	C,D	11.1 h	407.7	28.6	15
¹⁹⁵ Hg ^m	22.7 ±4.2	I	C,D	1.667 d	261.8	44.0	15
¹⁹⁷ Hg ^m	28.7 ±5.4	I	C	23.8 h	133.9	34.3	16
¹⁹⁷ Hg ^g	3.13 ±1.53	I	C	64.14 h	77.35	19.	16
¹⁹⁹ Hg ^m	8.63 ±.85	I	D	42.595 m	158.4	58.4	15
¹⁹² Tl	35.1 ±9.2	CD	C,D	10.7 m	274.8 ^f	46.1	15
¹⁹³ Tl	45.8 ±12.6	CD	C	21. m	255.6 ^g	7.	16
¹⁹⁴ Tl ^m	38.7 ±3.4	I	C,D	32.8 m	748.9	77.	16
¹⁹⁴ Tl	33.2 ±11.9	CD	C,D	35.107 m	645.5	13.0	15
¹⁹⁵ Tl	208. ±13.	I	C	1.16 h	884.5	3.6	15
¹⁹⁶ Tl ^m	88.0 ±5.1	I	C	1.410 h	426.3	92.	15
¹⁹⁶ Tl ^g	5.63 ±1.56	I	C	1.90 h	610.6	12.4	15
¹⁹⁷ Tl	52.9 ±3.7	I	C	2.837 h	308.5	4.36	16
¹⁹⁸ Tl ^m	16.3 ±1.5	I	C	1.870 h	282.8	27.	15
¹⁹⁸ Tl ^g	9.81 ±1.27	I	C	5.3 h	1420.6	8.0	15
¹⁹⁹ Tl	4.49 ±1.05	I	C	7.399 h	455.1	13.6	15
²⁰⁰ Tl	.324 ±.006	I	C	1.088 d	368.0	91.0	15
²⁰¹ Tl	.093 ±.013	I	C	73. h	167.4	8.0	15
²⁰² Tl	.030 ±.013	I	C	12.2 d	439.4	94.	15
¹⁹⁵ Pb	27.3 ±6.4	CD	D	17.006 m	383.5	93.5	15
¹⁹⁶ Pb	30.0 ±3.4	CD	C	36.994 m	425.7 ^f	87.2	15
¹⁹⁷ Pb ^m	23.3 ±1.6	CD	C	42.005 m	385.6	77.2	15
¹⁹⁸ Pb	7.48 ±1.58	I	C	2.4 h	365.4	32.	15
¹⁹⁹ Pb	4.71 ±1.01	CD	C,D	1.5 h	366.9	79.0	15
²⁰⁰ Pb	1.31 ±.25	I	C	21.499 h	147.6	28.3	15
²⁰¹ Pb	.252 ±.013	I	C	9.401 h	331.2	81.4	15
²⁰² Pb ^m	.085 ±.035	I	C	3.619 h	960.7	91.3	15
²⁰³ Pb	.006 ±.002	I	C	2.171 d	279.2	81.0	15
¹⁹⁸ Bi	6.29 ±.49	CD	D	11.85 m	1063.5	100.	15
²⁰⁰ Bi	.623 ±.143	CD	C	36.4 m	1026.	100.	16
²⁰¹ Bi	.127 ±.005	CD	C	1.8 h	331.2 ^f	81.4	15
²⁰² Bi	.030 ±.012	I	C	1.67 h	961.	100.	16
²⁰³ Bi	.016 ±.012	CD	C	11.8 h	820.	29.	16
²⁰⁴ Bi	.005 ±.002	I	C	11.2 h	899.	100.	16
¹⁹⁸ Po	.780 ±.100	I	RC	1.78 m	α (6.183	70.) ^h	16
¹⁹⁹ Po ^m	.183 ±.037	I	RC	4.2 m	α (6.060	39.) ^h	16
²⁰⁰ Po	.089 ±.020	I	RC	11.6 m	α (5.864	14.) ^h	16
²⁰² Po	.034 ±.012	CD	C	44. m	686.9	47.	16
²⁰⁴ Po	.016 ±.012	CD	C	3.52 h	1016.1	43.	17

a. I:Independent, CD:Partially cumulative from EC or β⁺, CR:Partially cumulative from β⁻.

b. C:Chemically separated, D:Non-destructive, RC:Rapid chemistry for α-counting.

c. Peak was observed, but large error.

d. Not corrected for ¹¹¹Pd^g.

e. ¹⁹³Hg^m/¹⁹³Hg^g=3 was assumed.

f. Obtained from daughter nuclide.

g. Obtained from grand-daughter nuclide.

h. α-energy in MeV.

TABLE 2. Isomer ratios ($\sigma_{\text{high spin}}/\sigma_{\text{low spin}}$) from the reaction of 240 MeV ^{12}C with ^{197}Au .

Nuclide	Spins	$\frac{\sigma_h}{\sigma_l}$, present work	$\frac{\sigma_h}{\sigma_l}$, other reactions
^{84}Rb	(6-), 2-	4.4 +- 2.5	
^{85}Sr	9/2+, 1/2-	28 +- 9	0.67 ^a (n_{th}, γ)
^{86}Y	8+, 4-	0.66 +- 0.59	0.45 ^b (p,p3n), $E_p=660$ MeV
^{116}Sb	8-, 3+	1.4 +- 0.6	2.03 +- 0.10 ^c ($\alpha, 3n$), $E_\alpha=32.3$ MeV
^{119}Te	11/2-, 1/2+	3.0 +- 0.8	2.70 +- 0.05 ^c ($\alpha, 3n$), $E_\alpha=33.4$ MeV
^{121}Te	11/2-, 1/2+	5.7 +- 2.1	2.00 +- 0.30 ^c ($\alpha, 3n$), $E_\alpha=33.4$ MeV
^{132}La	6-, 2-	2.3 +- 1.9	
^{160}Ho	5+, 2-	0.87 +- 0.70	
^{196}Au	12-, 2-	0.042 +- 0.011	0.054 +- 0.004 ^d (n,2n), $E_n=13.4$ MeV
^{198}Au	(12-), 2-	0.069 +- 0.023	
^{197}Hg	13/2+, 1/2-	9.2 +- 4.8	1.04 +- 0.15 ^e (d,2n), $E_d=21.4$ MeV
^{196}Tl	(7+), 2(-)	15.6 +- 4.4	
^{198}Tl	7+, 2-	1.66 +- 0.50	12 ^f ($\alpha, 3n$), $E_\alpha=35$ MeV

a. Reference 29

b. Reference 30

c. Reference 31

d. Reference 32

e. Reference 33

f. Reference 34

Figure Captions

1. Cross sections from the reaction of 240 MeV ^{12}C with ^{197}Au .

(a) Individual cross sections. Circles denote independent cross sections, triangles denote partially cumulative cross sections from β^+ or EC decay, and squares denote partially cumulative cross sections from β^- decay. Solid points denote the cross section for one-half of an isomer pair.

(b) The charge-dispersion-corrected mass distribution. The meanings of symbols other than circles for target-like products are described in the text. The full curve is a result of Gaussian fitting the fission products, and the dashed curve is that from Ref. 18 describing the fission distribution of 112 MeV $^{12}\text{C} + ^{197}\text{Au}$.

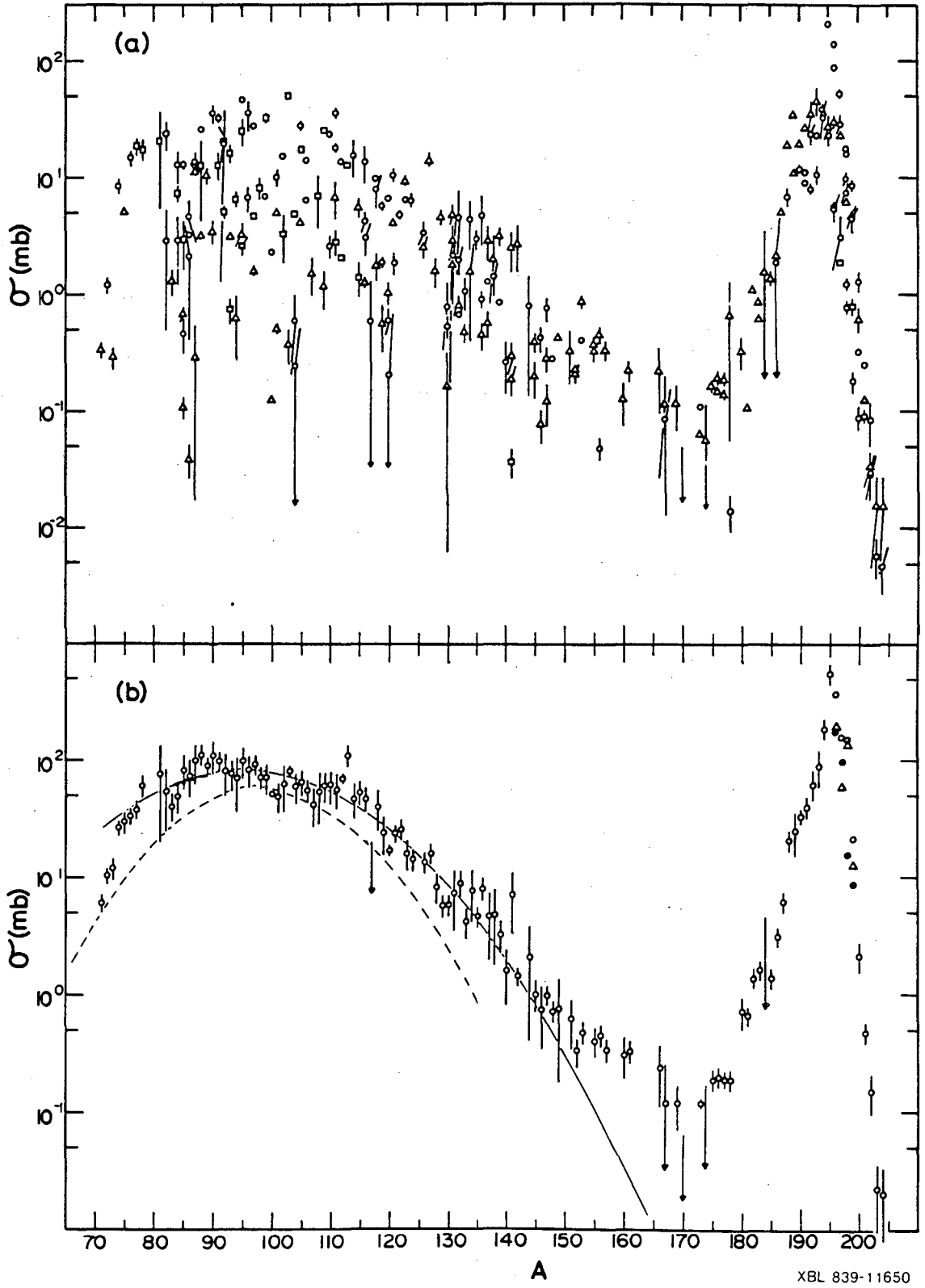
2. The cumulative charge dispersion of the fission products.

Circles denote independent cross sections, triangles denote partially cumulative cross sections from β^+ or EC decay, and squares denote partially cumulative cross sections from β^- decay.

3. The charge dispersions of target-like products for $A = 196$ to $A = 204$. Circles denote independent cross sections, triangles denote partially cumulative cross sections from β^+ or EC decay, and squares denote partially cumulative cross sections from β^- decay. Solid points denote the cross section for one-half of an isomer pair.

4. The dependence of the isotopic distribution of high Z products on Q_{gg} . The calculation of Q_{gg} in this case is discussed in the text. Circles denote independent cross sections, triangles denote partially cumulative cross sections from β^+ or EC decay, and squares denote partially cumulative cross sections from β^- decay.

5. The isotopic distributions of target-like products. Z refers to the atomic number of the target nucleus (79). Circles denote independent cross sections, triangles denote partially cumulative cross sections from β^+ or EC decay, and squares denote partially cumulative cross sections from β^- decay. Solid points denote the cross section for one-half of an isomer pair.



XBL 839-11650

Fig. 1

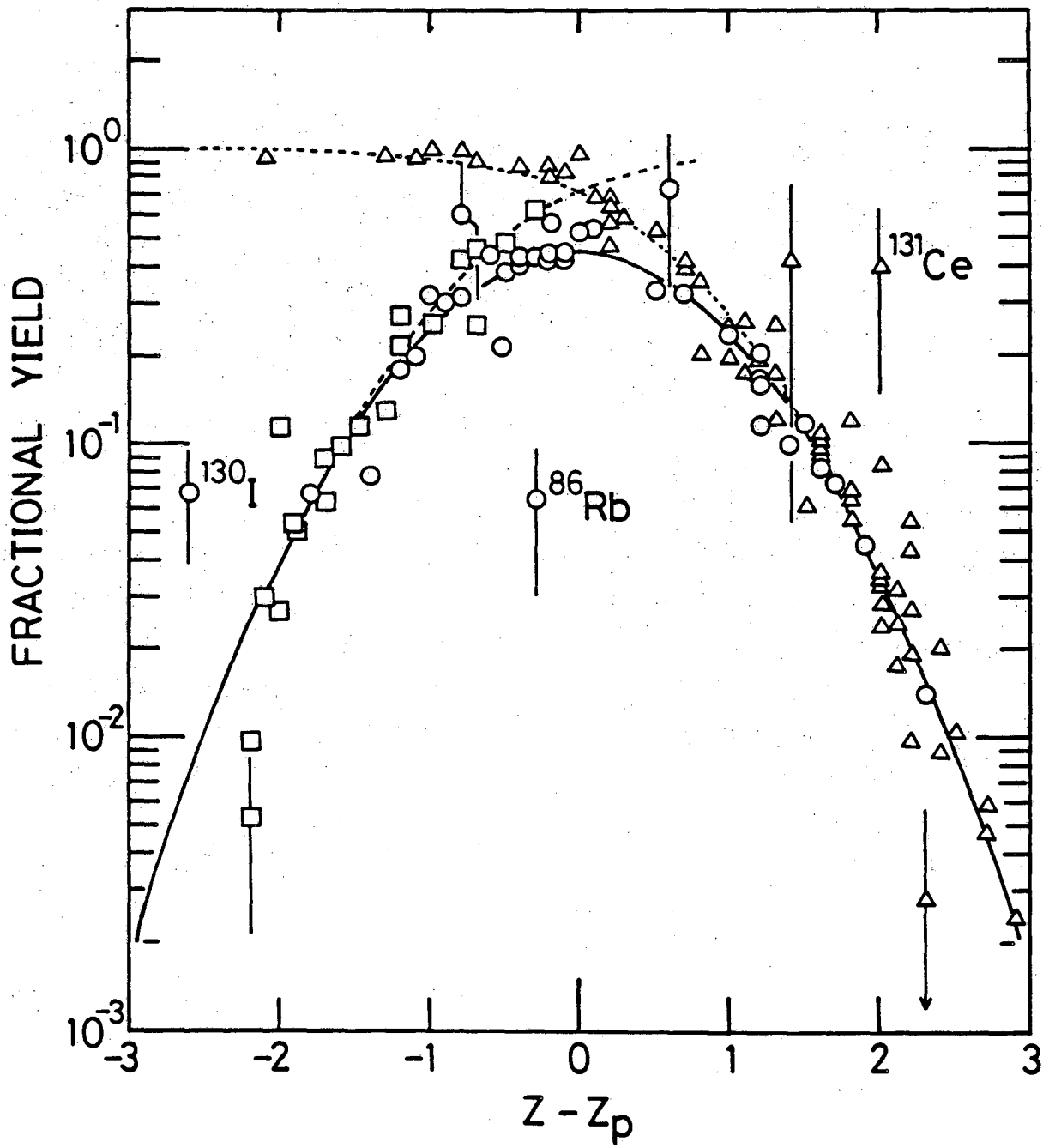


Fig. 2

XBL 839-11649

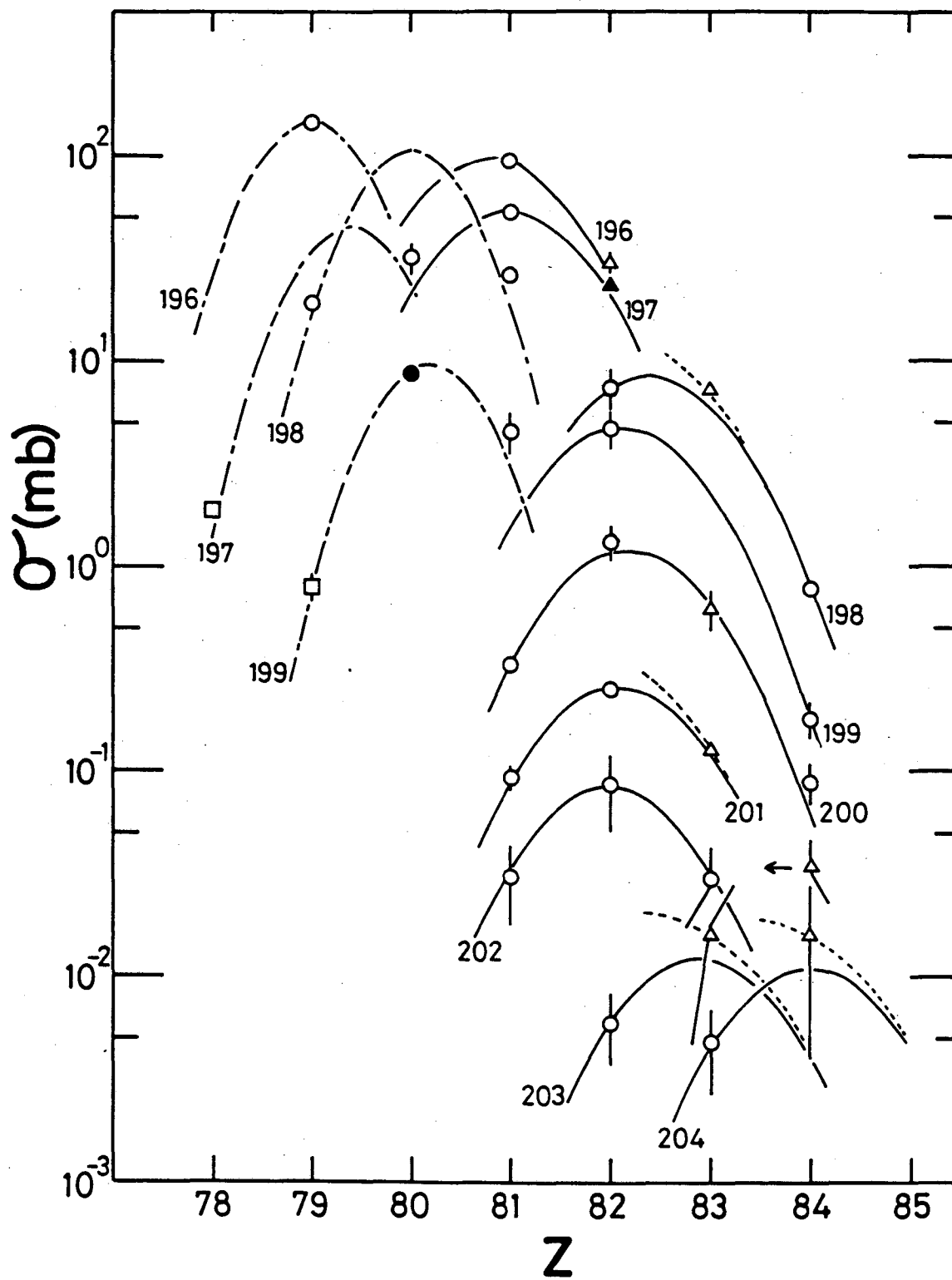


Fig. 3

XBL 839-11648

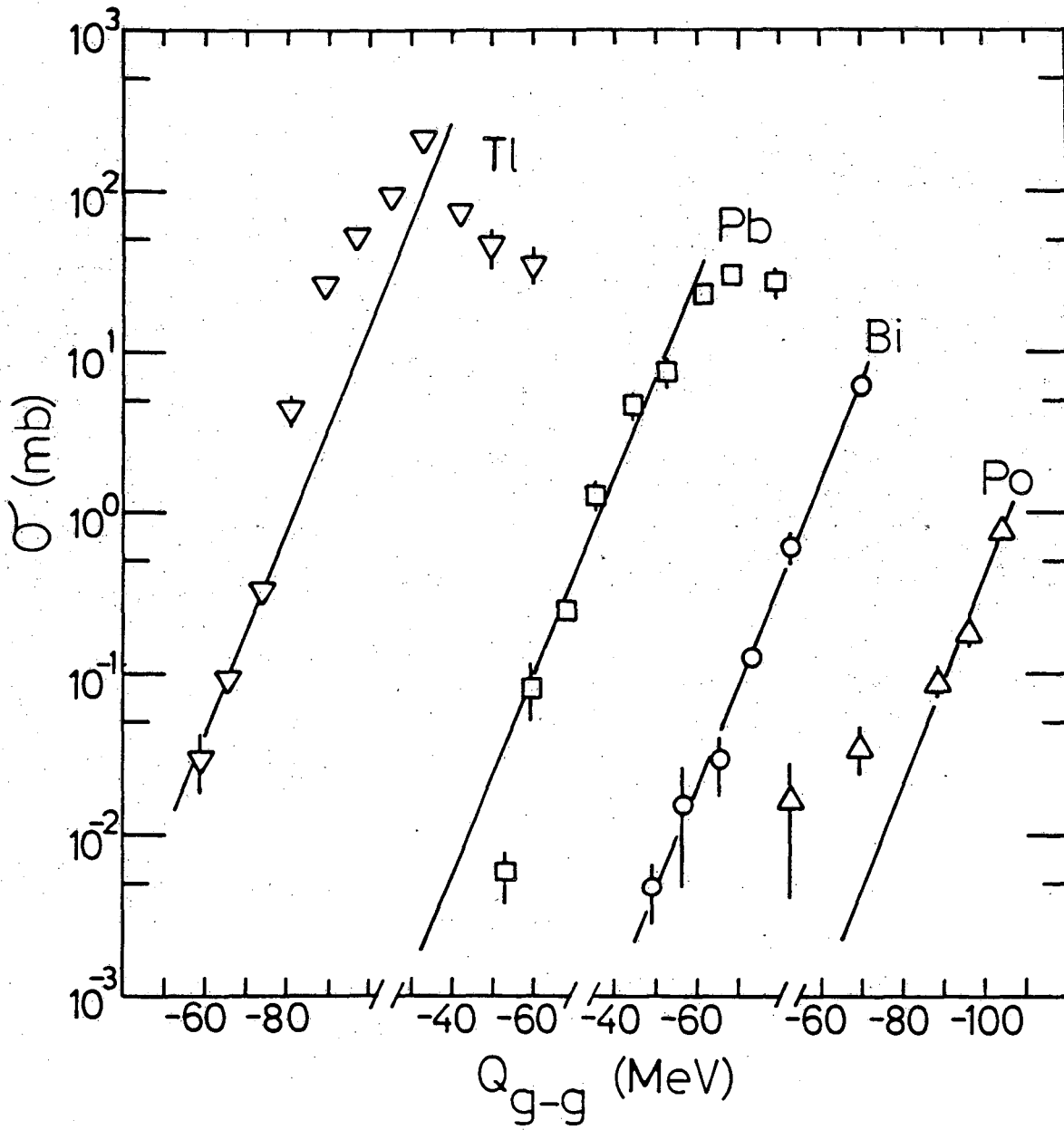


Fig. 4

XBL 339-11646

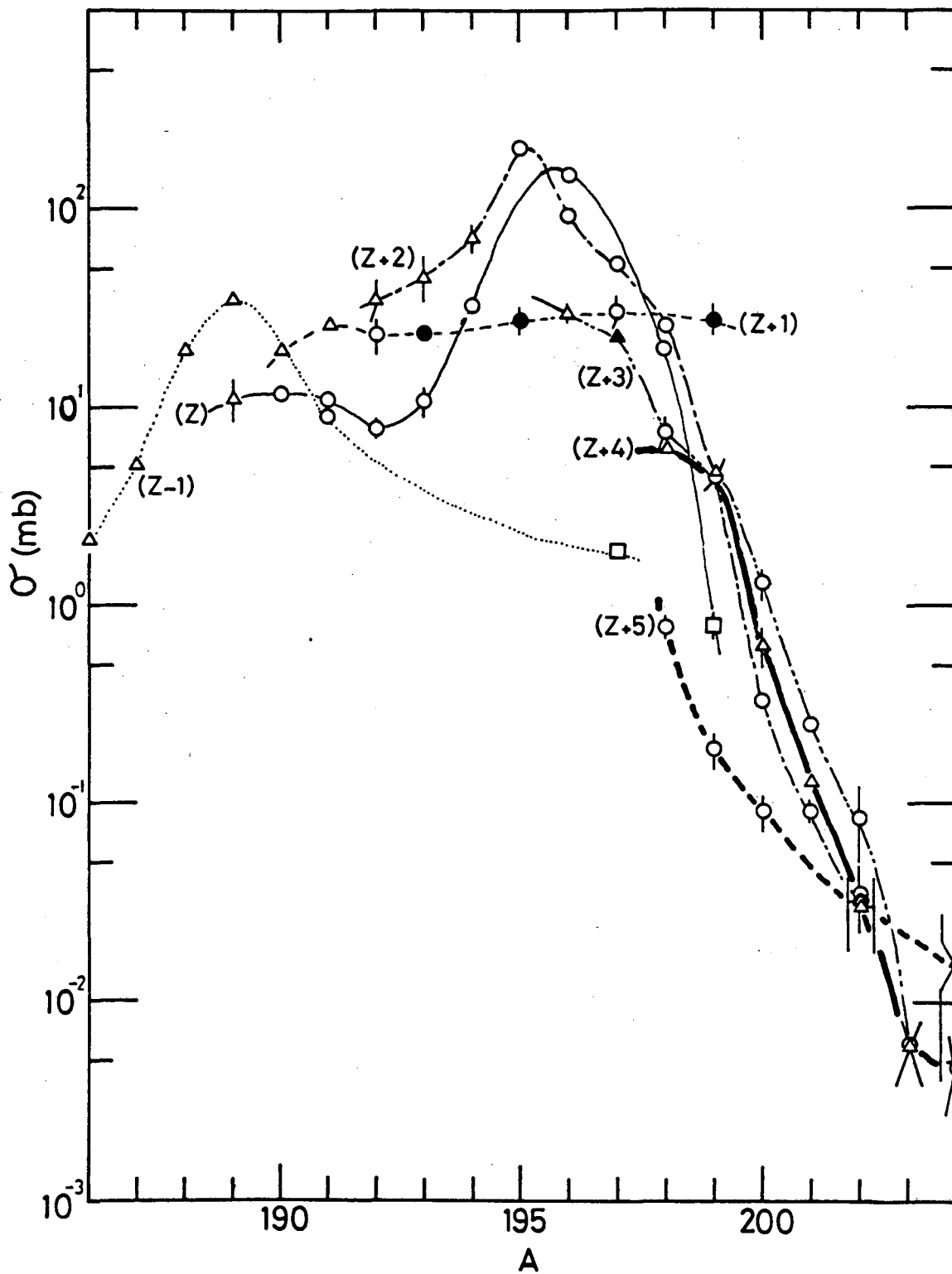


Fig. 5

XBL 839-11647

This report was done with support from the Department of Energy. Any conclusions or opinions expressed in this report represent solely those of the author(s) and not necessarily those of The Regents of the University of California, the Lawrence Berkeley Laboratory or the Department of Energy.

Reference to a company or product name does not imply approval or recommendation of the product by the University of California or the U.S. Department of Energy to the exclusion of others that may be suitable.

TECHNICAL INFORMATION DEPARTMENT
LAWRENCE BERKELEY LABORATORY
UNIVERSITY OF CALIFORNIA
BERKELEY, CALIFORNIA 94720